J. Fluid Mech. (2006), *vol.* 560, *pp.* 53–64.
doi:10.1017/S0022112006000292 Printed in the United Kingdom

Simultaneous orthogonal-plane particle image velocimetry measurements in a turbulent boundary layer

By W. T. HAMBLETON, N. HUTCHINS AND IVAN MARUSIC

Department of Aerospace Engineering and Mechanics, University of Minnesota, Minneapolis, MN 55455, USA

(Received 13 July 2005 and in revised form 25 November 2005)

Stereoscopic particle image velocimetry (PIV) measurements were taken simultaneously in streamwise–spanwise and streamwise–wall-normal planes in a zero-pressure-gradient turbulent boundary layer over a flat plate. Polarization techniques were employed to allow PIV to be taken in both planes simultaneously. Image preprocessing techniques were used to improve the quality of data near the line of intersection of the planes. Linear stochastic estimation was performed on these data, revealing the streamwise, spanwise, and wall-normal extent of swirl events primarily near the top of the log region of the boundary layer. Swirl events with rotation consistent with the mean vorticity are found to have a large footprint in the lower limit of the log region whereas swirls with opposite-signed vorticity are found to have little influence lower in the boundary layer. These long-time-averaged statistics contain features that are consistent with the hairpin packet model (or its kinematic equivalent). This model also seems to provide a reasonable description of many instantaneous events involving large-scale coherence, where long regions of streamwise momentum deficit are surrounded by vortex cores.

1. Introduction

One of the more active areas of contemporary research in turbulent boundary layers has been the development of models composed of a series of kinematic events that have some organization and coherence in space and time. Many workers have focused their efforts on understanding the morphology, characteristics, and dynamical behaviour of these events, collectively referred to herein as coherent structures or coherent events. While the behaviour of the viscous sublayer and buffer layer have been extensively studied for some time, and is described well by a near-wall cycle involving quasi-streamwise vortices, the understanding of coherent events in the log and wake regions has had to await more recent developments in experimental particle image velocimetry (PIV) and direct numerical simulation (DNS) procedures. One of the more striking features of these regions are the long zones of streamwise momentum deficit with spatial scales proportional to the boundary layer thickness.

Several workers have analysed time-averaged statistics and instantaneous fields and found evidence of large structures. Adrian, Meinhart & Tomkins (2000*b*) investigated the organization of coherent events of large streamwise extent in the streamwise–wall-normal plane (hereinafter called the vertical plane), which led them to propose

the hairpin packet model for coherent motions. Christensen & Adrian (2001) looked at similar events and highlight their structure using stochastic estimation, finding evidence of arrays of vortices which grow in wall-normal extent from upstream to downstream. Ganapathisubramani, Longmire & Marusic (2003) investigated the Reynolds shear stress associated with events with large streamwise coherence in the streamwise–spanwise plane (hereinafter called the horizontal plane) and find that these large events are some of the primary contributors to Reynolds stress in wall turbulence. Tomkins & Adrian (2003) investigated the organization of these events and studied how their characteristic spanwise dimensions behave at different wall-normal locations through the boundary layer using linear stochastic estimation. With all these analyses, however, there is some room for speculation about the three-dimensional structure of large coherent motions.

In an effort to achieve a more three-dimensional view of large coherent events, Ganapathisubramani *et al.* (2005) and Hutchins, Hambleton & Marusic (2005) investigate the shape and spatial extent of events in the log and wake regions using time-averaged statistics and infer the spatial scales from the shape of contours of two-point correlations. These results are, however, limited to presenting contours on a set of planes which mutually intersect a condition point and present little insight into the three-dimensional shape of instantaneous realizations of coherent motions. DNS data are, of course, a means of obtaining full three-dimensional information in a turbulent flow, and has been used by many workers. Jiménez & del Álamo (2004) and del Álamo *et al.* (2004, 2006) have analysed large-scale features in DNS of channel flow at a Reynolds number comparable to the present data and find similar results in the instantaneous structure of these events. They interpret the large-scale low-momentum regions as 'wakes' behind vortex clusters which spread under the effect of the background turbulence, very different from the model of Adrian *et al.* (2000*b*) whereby hairpin vortices form groups called 'packet' as a result of an autogeneration mechanism.

In an effort to obtain a three-dimensional instantaneous view from experiments we undertook the present work, wherein a vertical plane of PIV is taken simultaneously with a horizontal plane. Recently, and unknown to us through much of this work, Kim & Kwon (2004) have performed this measurement at a Kármán number of up to 526, although there are differences in image preprocessing between that work and ours. The main obstacle in this experiment was extinguishing the images of particles not in the plane of interest. The work of Kim & Kwon as well as this work utilizes polarization to solve much of this problem. In addition, we also here use a background subtraction technique that seems to solve the remainder of the light contamination problem (described in § 2).

The data presented here are primarily used to provide a qualitative picture of large-scale coherent events in the turbulent boundary layer. We consider instantaneous three-dimensional results, as well as time-averaged statistics using LSE (linear stochastic estimation). The utility of the simultaneous combined planes is to enable a condition point for three-dimensional statistics that does not necessarily reside on the intersection of the planes. This helps to describe the extent to which events in the wake region influence statistics in the log region. The present data set (and any other static data result) is capable only of elucidating instantaneous fields and not a dynamical mechanism. Amongst other things, these data can be used to further refine structure-based shot noise models as in Perry & Marusic (1995) and Marusic (2001). The flow patterns seen from the LSE (see figure 6) can be used as the starting point for the vortex skeletons used in such models.

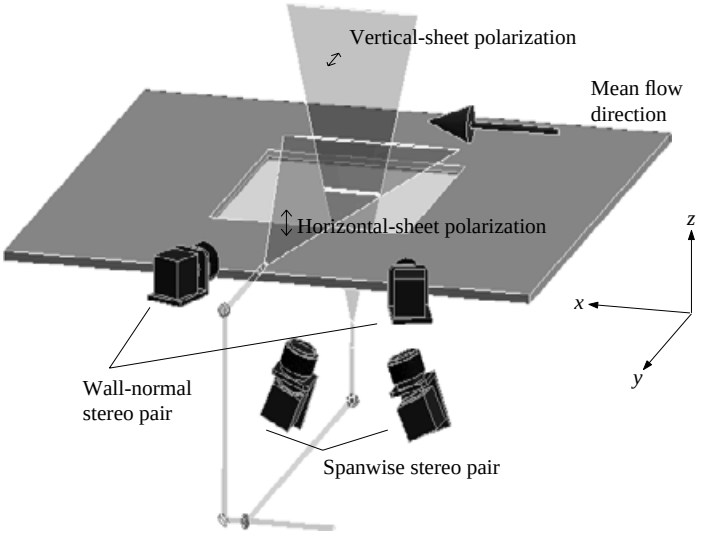

FIGURE 1. Depiction of experimental configuration.

2. Experiments and data processing

The free-stream velocity during the experiment was $6.0\,\mathrm{m\,s^{-1}}$ yielding a boundary layer thickness δ, measured by fitting the profile to the wake function presented by Lewkowicz (1982), of 68 mm. Skin friction velocity, u_τ, was determined by a Clauser chart and found to be $0.25\,\mathrm{m\,s^{-1}}$, making the Kármán number, $Re_\tau = \delta\tau/\nu = 1100$, where ν is the kinematic viscosity of the fluid. The momentum-thickness Reynolds number, R_θ, was 2600. The horizontal plane was taken nominally in the log region at $z^+ = 98$ ($z/\delta = 0.08$). Here x, y and z denote the streamwise, spanwise and wall-normal directions respectively, and the superscript + indicates normalization with wall variables (u_τ and ν/u_τ.)

The flow was seeded with olive oil particles generated by a bank of Laskin nozzles and nominally 1 μm in diameter, as described in Raffel, Willert & Kompenhans (1998). The light source was a Spectra Physics PIV400 Nd:YAG laser emitting 0.532 μm radiation. Two orthogonal, intersecting planes of particles were illuminated, with their line of intersection in the streamwise direction. The two light sheets are formed by splitting one beam into two, then sending each of these through its own set of spherical and cylindrical lenses. A schematic of the optical setup is shown in figure 1. The stereoscopic angle (or angle from the measurement-plane normal vector to the optical axis of the camera) on both sets of cameras was 18°.

Images were processed using an unmodified version of TSI's Insight 6.1. The vertical-plane images were taken using TSI Pivcam 10–30 one megapixel cameras. Velocity vectors for these images were obtained using 16 pixel square interrogation spots with 50% overlap, with correlations performed by zero padded FFT and three-point Gaussian subpixel interpolation. The horizontal plane images were taken with TSI Powerview 4 megapixel cameras. Processing for this plane was performed with 20 pixel square interrogation spots but otherwise the same settings as for the vertical cameras. Interrogation spot sizes were chosen as a compromise between the spatial resolution and spatial extent of images. Interrogation spot size is 32 wall units square for the vertical plane and 35 wall units square for the horizontal.

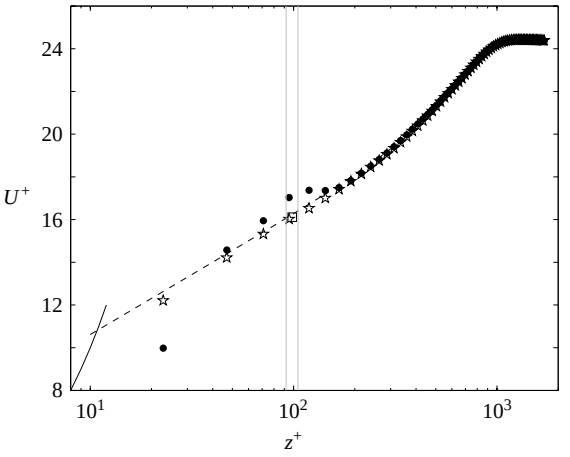

FIGURE 2. The effect of background subtraction on mean velocity. Dashed line is the log law with $\kappa = 0.41$, $A = 5.0$ and the wake profile of Lewkowicz (1982), solid line is $U^+ = z^+$, filled circles are measured mean velocity without background image subtraction, the square is horizontal-plane data with background subtraction, and stars are measured mean velocity with background image subtraction. The location and thickness of the horizontal sheet is marked with vertical lines.

The two light sheets have different polarizations, allowing the use of polarizing filters on the cameras to separate out illuminated particles not in the light sheet of interest. The seeding particles are small enough and the incident light polarization is such that the polarization of the light scattered to each camera pair is nearly orthogonal between the two different planes, as noted in a description of polarization techniques applied to multiple plane PIV by Kähler & Kompenhans (2000). Although much of the light from particles in the other plane is extinguished, it is never fully eliminated due to the quality of the filters used and the uniformity of the incident polarization. A modicum of image preprocessing must be used to recover particle details at the intersection. The small fraction of light from the other plane that is allowed into the camera is enough to cause problems with accuracy of measurement near the intersection of the two planes. Illuminated particles which are far out of focus cause a background glow which is nearly constant from frame to frame. There are several possible reasons why this would affect the accuracy of the cross-correlation algorithm, but they will not be discussed here. The image preprocessing used here was to create a mean image made by averaging 100 or so individual images and subtracting the result from each individual image, thus removing any persistent bright spots. Plots of mean statistics with and without this background subtraction are shown in figures 2 and 3. A total of 1500 frames were acquired. For reference, these data are plotted against those of Spalart (1988) for $R_\theta = 1410$. Note the poor performance of statistics from the uncorrected PIV near the line of intersection without the ensemble image subtraction and the dramatically improved performance with subtraction. The remaining discrepancy between these statistics and those measured by other means in the near-wall region reflects the spatial resolution limits of the present PIV setup (Hutchins *et al.* 2005).

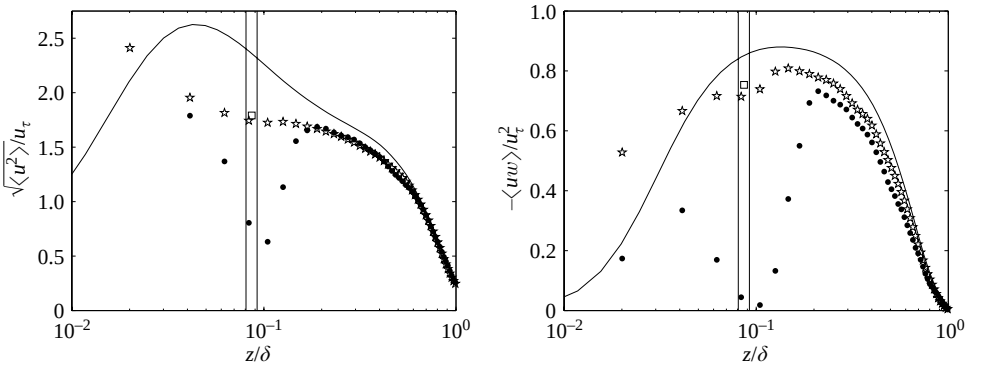

FIGURE 3. Effect of background subtraction on turbulence intensity and Reynolds shear stress: solid line, DNS data of Spalart (1988); filled circles, measured quantities without background image subtraction; stars, measured quantities with background image subtraction; square, horizontal plane data after background subtraction. The location and thickness of the horizontal sheet is marked with vertical lines.

3. Results

In this section results from instantaneous realizations will be considered followed by statistically averaged results using linear stochastic estimation (LSE).

3.1. *Example instantaneous field*

Quantities from an instantaneous field are shown in figure 4. The frame is selected such that an elongated low-momentum streak lies on the intersection of the vertical and horizontal planes, and the results are typical of those observed in many realizations where such an intersection occurred. Figures 4(*a*), 4(*b*) and 4(*d*) show the fluctuating streamwise velocity while 4(*c*) and 4(*e*) show the associated magnitude of the signed swirl, λ. Swirl is defined as the imaginary part of the eigenvalue of the velocity gradient tensor (for the present data set the tensor is two-dimensional), and has been shown to be a good identifier of vortex cores. For a detailed description of swirl and its interpretation, see Adrian, Christensen & Liu (2000*a*). Signed swirl is obtained by multiplying swirl by the sign of the out-of-plane component of vorticity.

In figure 4 the horizontal-plane results (b, c) are typical of those reported by Ganapathisubramani *et al.* (2003) and Tomkins & Adrian (2003), where the low-speed regions are flanked by positive signed swirls in the negative spanwise direction and negative signed swirls in the positive spanwise direction. Similarly the vertical-plane results (figure 4d, e) are typical of those reported by Adrian *et al.* (2000*b*) with the low-speed region primarily surrounded from above by a series of positive signed swirl patches.†

The observed arrangements of vortex cores surrounding the low-momentum region are consistent with the hairpin packet paradigm with the caveat that any hairpin vortices that do exist are likely to be far from symmetric or two-sided in an instantaneous case. For any turbulent flow symmetric two-sided vortex structures

† Note, that the actual signs of swirl will be opposite to Adrian *et al.* (2000*b*) because of the different right-handed coordinate systems used. Here we use z as the wall-normal direction and hence the mean spanwise vorticity is positive.

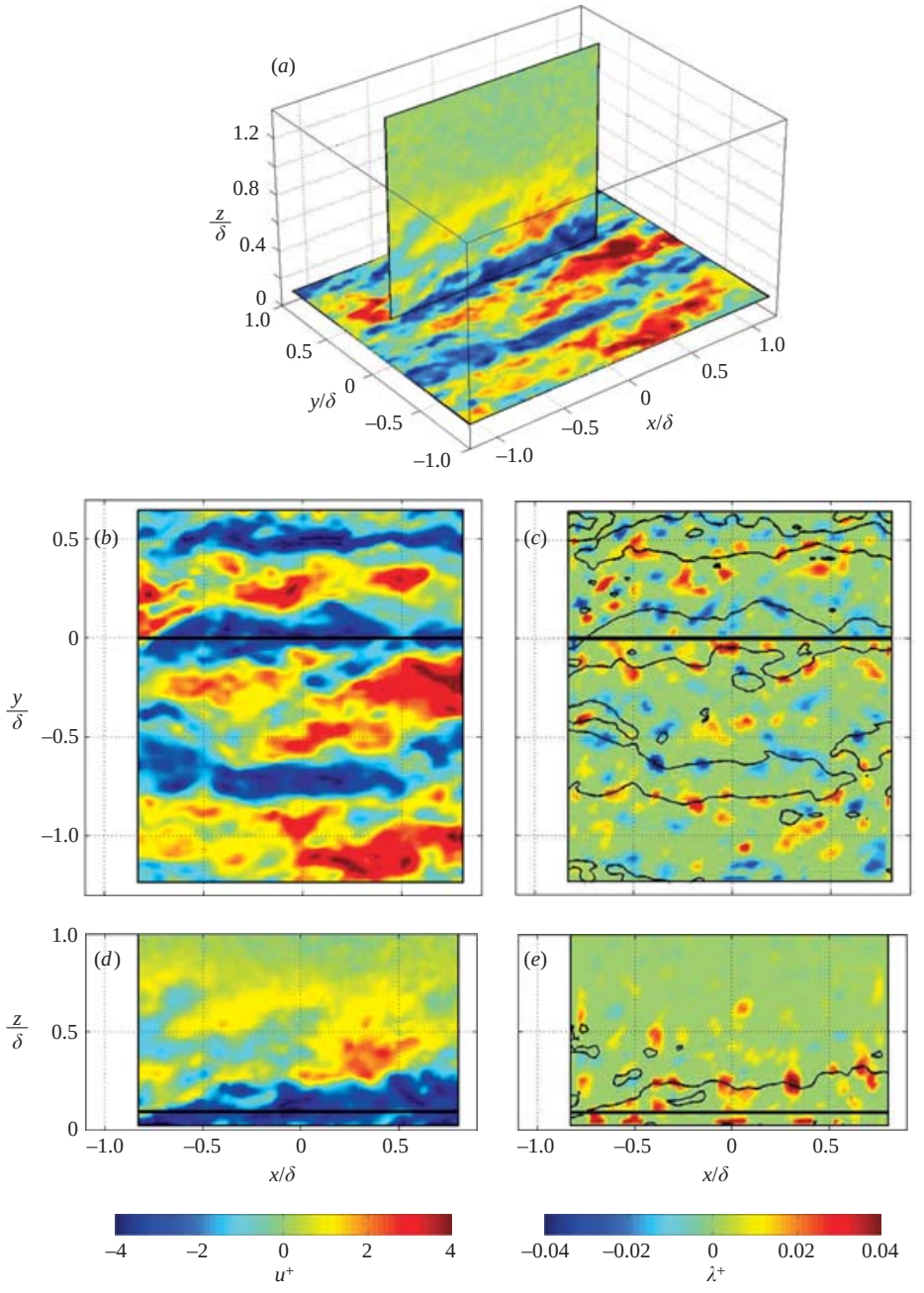

FIGURE 4. (*a*) Three-dimensional view of both orthogonal planes; (*b*, *c*) plan-view of horizontal plane and (*d*, *e*) side-view of vertical plane for example instantaneous flow field. Plots (*a*, *b*, *d*) show streamwise velocity fluctuations u^+. Plots (*c*, *e*) show instantaneous signed swirl with iso-contours of $u^+ = -1$ superimposed in black. Colour scale indicates fluctuation magnitude.

are only to be expected in a time-averaged sense. It should be emphasized that the term 'hairpin packet' as used here applies only in a kinematic sense and simply refers to the clustering of vortex structures about a region of low momentum. No

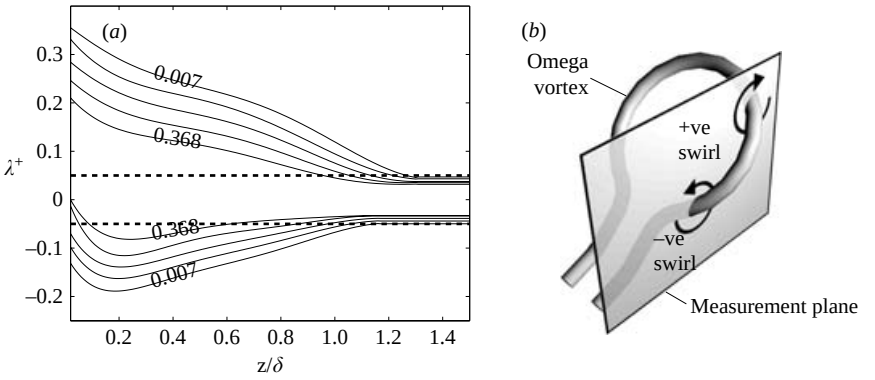

FIGURE 5. (*a*) Probability density function (p.d.f.) of signed swirl at a given height. Contours show normalized PDF and are logarithmically spaced from 0.007 to 0.368. (*b*) Schematic of one possible origin of vorticity contrary to the mean vorticity in the vertical plane.

inference about the dynamics or any cause-and-effect arguments can be made from these instantaneous data.

The observed low-speed region highlighted in figure 4 exceeds the field of view of 2δ in the streamwise direction, and evidence in the literature suggests that it could be significantly longer (see for example Kim & Adrian 1999; del Alamo *et al.* 2004; Hutchins, Ganapathisubramani & Marusic 2004). The wall-normal extent of the low-speed region is seen to increase in the downstream direction, consistent with two-point correlation contour results obtained by various investigators, including Kovasznay, Kibens & Blackwelder (1970), Christensen & Adrian (2001) and Ganapathisubramani *et al.* (2005). The spanwise extent of the low-speed region, in these instantaneous views, exhibits no notable spread in either the downstream or upstream directions.

Note also in figure 4 (roughly at $x/\delta \approx -0.5$, $z/\delta \approx 0.25$) that there is a negative swirl event (a swirl which is associated with rotation contrary to the direction of the mean vorticity), which is associated with a small region of low-speed fluid above it and a positive swirl above that. This event would be consistent with either a severely omega-shaped vortex loop, shown schematically in figure 5(*b*), or possibly a vortex ring. This event is quite weak and stronger ones do occur, and while such events are far from being statistically dominant they do occur fairly frequently, witnessed in a plot of the signed swirl p.d.f., figure 5. It can also be seen by looking at many of the negative signed swirl events that the spatial extent of the velocity field coherence is not particularly large and that it typically extends to higher rather than lower wall-normal positions. Some of the characteristics and ramifications of motions of this type have been discussed by Klewicki (1997).

3.2. *LSE*

Data were also processed using linear stochastic estimation (LSE), similar to results presented for the vertical plane in Christensen & Adrian (2001). A very thorough derivation of LSE, as well its properties as they pertain to fluid mechanics, can be found in Adrian & Moin (1988). LSE is an estimate of the true conditional average based upon unconditional two-point spatial correlations. Here we use two distinct condition vectors: positive signed swirl (λ_p) and negative signed swirl (λ_n). (Here λ_p

is equal to signed swirl λ only where $\lambda > 0$, similarly λ_n is equal to λ where $\lambda < 0$.) Thus, the LSE for λ_p is

$$\langle u_j(\boldsymbol{x}+\boldsymbol{r})|\lambda_p(\boldsymbol{x})\rangle = \frac{\langle \lambda_p(\boldsymbol{x})u_j(\boldsymbol{x}+\boldsymbol{r})\rangle}{\langle \lambda_p(\boldsymbol{x})\lambda_p(\boldsymbol{x})\rangle}\lambda_p(\boldsymbol{x}). \tag{3.1}$$

Two-point correlations are calculated directly between the condition vector and the velocities. For example, the correlation coefficient between positive swirl and streamwise velocity for the vertical plane is defined as

$$R_{\lambda_p u}(\Delta x, z) = \frac{\langle \lambda_p(x, z_{ref})u(x+\Delta x, z)\rangle}{\sigma_{\lambda_p}(z_{ref})\sigma_u(z)} \tag{3.2}$$

where σ is the root-mean square of a given quantity, z_{ref} is the wall-normal height where the condition event is considered, and angled brackets indicate ensembled results over all the available frames.

Swirl is chosen for the condition vector for the stochastic estimation because of its compactness, as a result of which phase jitter will be kept to a minimum and only data associated with that particular event will contribute to the stochastic estimate. This is different from conditioning on, say, velocity, where many different types of events can produce the same velocity at a point.

Owing to the noise in measurement, signed swirl is thresholded at $\lambda^+ = \pm 0.05$ to yield clearer results. The threshold was chosen to eliminate residual noise, visible in the p.d.f. of swirl in the free-stream as shown in figure 5. The qualitative behavior of LSEs with and without the thresholding is the same (because low-amplitude swirl is mostly noise), but the thresholding provides a slightly cleaner result.

The result shown in figure 6 is the direction field (all vectors set to unit magnitude) for the linear stochastic estimate of a positive swirl event at $z/\delta = 0.19$. The direction field in the vertical plane exhibits features similar to those presented in Christensen & Adrian (2001) for turbulent channel flow, with a strong swirl at the condition point (marked with a cross) and a 'packet angle' (Adrian *et al.* 2000*b*) of approximately 13°. The unique feature of the current result is provided by the simultaneous view given by the horizontal plane of figure 6(*b*). A clear large-scale coherence is noted with the condition event in the vertical plane being accompanied by two pronounced swirling motions that occur just upstream of the condition point at $\Delta y \approx \pm 0.15\delta$. This indicates that the time-averaged conditional event is an inclined hairpin structure, with an inclination angle of close to 45°. Between the legs of this conditional eddy, there is a pronounced elongated low-speed region extending some distance up- and downstream of the condition point. This structure seems to widen with increasing Δx and is flanked in y by high-speed regions. Some evidence of secondary swirling activity is noted at the shear layer between these low- and high-speed regions. For this statistical field, all of these features bear a strong resemblance to a hairpin packet structure. Alternative explanations have been proposed to explain such time-averaged features. For example, the widening of the low-speed region in figure 6(*b*) is consistent with a spreading 'wake' as proposed by Jiménez & del Álamo (2004), although we feel that this is more likely explained by a meandering of the low-speed regions (Hutchins *et al.* 2004).

A further interesting feature in the horizontal plane of figure 6(*b*) is the saddle point that seems to occur at $\Delta x \approx -0.57\delta$. This feature corresponds to the point in the side view (plot *a*), where the inclined shear layer crosses the horizontal measurement plane ($z/\delta \approx 0.09$). Again, such saddle points would be predicted by the inclined hairpin

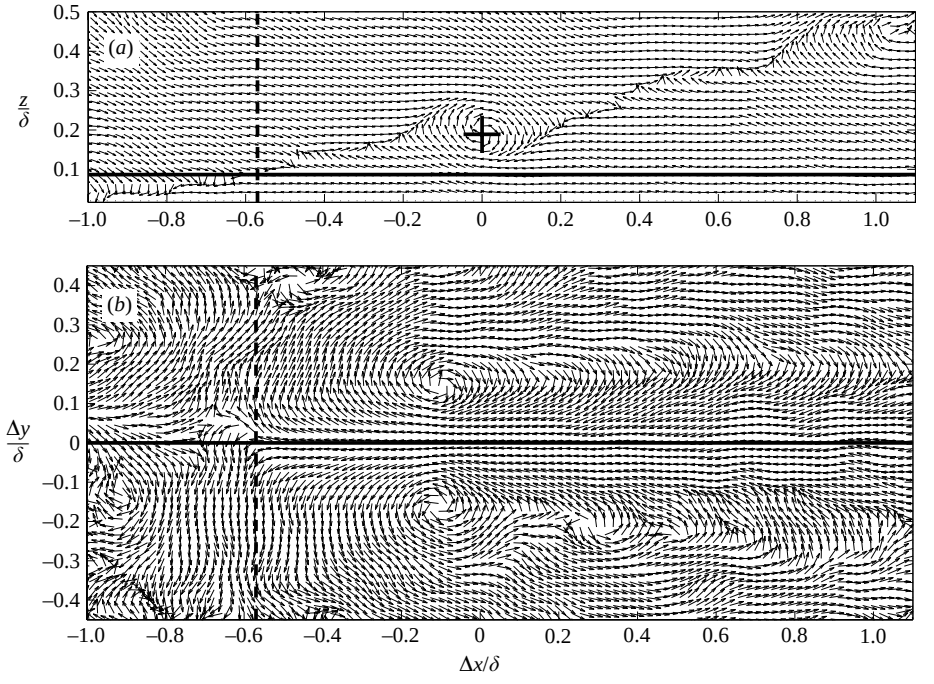

FIGURE 6. Direction field from linear stochastic estimation of velocity based on positive signed swirl (swirl consistent with mean vorticity) at $z_{ref}/\delta = 0.19$. The vertical plane is shown in (*a*), with the condition point marked with a cross, and the horizontal plane is shown in (*b*).

packet scenario if the heads of the smallest hairpin structures (at the upstream end of the packet) were below the wall-parallel measurement plane.

It is also worth noting that similar results are obtained even if the condition point is higher in the wake region, though the streamwise coherence, particularly in the horizontal plane, is somewhat diminished. Concerning the interpretation of the direction fields shown, we believe that the regions in which the direction field is organised (or the two point correlations are converged) represents the scale of the average spatial coherence of a given event. The rationale is that if many events of a similar size and shape are present, then the correlations will converge faster in those regions compared to outside where the kinematics become random compared to the condition point. When viewing the entire spatial extent of the direction field that can be generated (only part of it is shown in figure 6), the spatial extent of the coherence seems to manifest itself through a sudden change from regions where the direction field is constant or slowly changing to where it is completely random.

It is also of interest here to consider an LSE based on negative swirl in the vertical plane (opposite to the sign of $\partial U/\partial z$), and this is shown in figure 7. In this case a smaller number of candidate events exist, and consequently the statistics are not as well converged (even with the 1500 frames used). Ideally further studies with a considerably larger number of frames are required. However, as a preliminary result, an interesting feature seems to emerge in the vertical plane, with an associated clockwise spinning swirl event appearing above and downstream of the condition point, consistent with an omega-shaped vortex or vortex ring structure (see figure 5*b*). Falco (1991) observed vortex ring structures (so-called typical eddies) that spanned

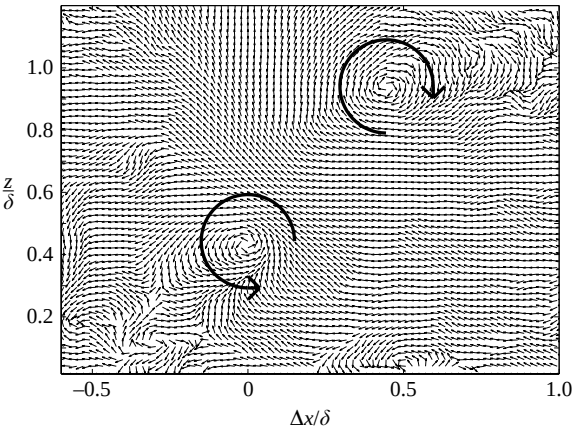

FIGURE 7. Direction field from linear stochastic estimation of velocity based on negative signed swirl (swirl counter to the mean vorticity) at $z_{ref}/\delta = 0.44$.

a substantial portion of δ at low Reynolds number ($Re_\theta = 753$). However, it was suggested that overall these structures have a size that is of the same order as the Taylor microscale (with a weak Reynolds number dependence) yielding a length scale of approximately 60–70 viscous wall units. This equates to 0.06δ for the present experiments, which is clearly much smaller than the structure implied by figure 7. Kiger & Pan (2002) also show instantaneous examples of counter-rotating spanwise vortices of the form given by figure 7.

The result in figure 7 is dependent on the z_{ref} chosen. For small values of z_{ref} close to the horizontal plane, the results are relatively trivial with the LSE just returning the candidate event (i.e. a negative vortex core in the vertical plane and no substantial imprint on the horizontal plane). The z_{ref} chosen for figure 7 is representative of the outer wake region. Contrary to the positive swirl case of figure 6, the majority of correlated behaviour seems to take place above z_{ref}/δ for the negative signed event, and no significant spatial coherence is found in the horizontal plane (unless z_{ref}/δ is small enough such that the horizontal plane bisects the candidate event). The lack of footprint below these structures and the z_{ref} at which they emerge (onset of the wake region) is consistent with the lifted or detached wake-type structures discussed by Perry & Marusic (1995) and Hutchins *et al.* (2005).

4. Conclusions

In this paper, PIV data taken simultaneously in streamwise–spanwise and streamwise–wall-normal plane are presented. The PIV technique relies on light sheet polarization as well as image preprocessing techniques in order to obtain measurements near the line of intersection of the two PIV planes. A representative instantaneous field is presented where both frames intersect a large elongated region of momentum deficit. Patches of swirl (of appropriate sign) are found to largely reside around the region of momentum deficit in both planes.

Time-averaged statistics, in the form of linear stochastic estimation, are presented and show shapes and extents consistent with the representative instantaneous field, indicating that such features occur relatively frequently and with approximately similar structure. However, it must be kept in mind that any conditionally averaged result contains an imposed spanwise symmetry that need not necessarily reflect any

instantaneous events. The LSE result, based on a condition of positive swirl in the vertical plane, slightly above the log region, shows an average three-dimensional structure that is consistent with the hairpin packet model. Additional time series or Lagrangian data are needed to conclusively comment on any dynamic formation mechanisms (e.g. autogeneration) that have been associated with this model (Adrian *et al.* 2000*b*). The present data are limited to a purely kinematic representation. Preliminary results are also presented with regard to swirl events associated with vorticity counter to the mean shear, and it is conjectured that if these events have any dominant organization it would be in the form of vortex rings or omega-shaped vortex loops.

The authors gratefully acknowledge support from the National Science Foundation (Grant CTS-0324898) and the David and Lucile Packard Foundation. We are indebted to B. Ganapathisubramani for his help with experimental setup and many useful discussions during the course of this study.

REFERENCES

Adrian, R. J., Christensen, K. T. & Liu, Z. C. 2000*a* Analysis and interpretation of instantaneous turbulent velocity fields. *Exps. Fluids* **29**, 275–290.

Adrian, R. J., Meinhart, C. D. & Tomkins, C. D. 2000*b* Vortex organization in the outer region of the turbulent boundary layer. *J. Fluid Mech.* **422**, 1–54.

Adrian, R. J. & Moin, P. 1988 Stochastic estimation of organized turbulent structure: homogeneous shear flow. *J. Fluid Mech.* **190**, 531–559.

del Álamo, J. C., Jimenez, J., Zandonade, P. & Moser, R. D. 2004 Scaling of the energy spectra of turbulent channels. *J. Fluid Mech.* **500**, 135–144.

del Álamo, J. C., Jimenez, J., Zandonade, P. & Moser, R. D. 2006 Self-similar vortex clusters in the turbulent logarithmic region. *J. Fluid Mech.* (in press).

Christensen, K. T. & Adrian, R. J. 2001 Statistical evidence of hairpin vortex packets in wall turbulence. *J. Fluid Mech.* **431**, 433–443.

Falco, R. E. 1991 A coherent structure model of the turbulent boundary layer and its ability to predict Reynolds number dependence. *Phil. Trans. R. Soc. Lond.* A **336**, 103–129.

Ganapathisubramani, B., Hutchins, N., Hambleton, W. T., Longmire, E. K. & Marusic, I. 2005 Investigation of large-scale coherence in a turbulent boundary layer using two-point correlations. *J. Fluid Mech.* **524**, 57–80.

Ganapathisubramani, B., Longmire, E. K. & Marusic, I. 2003 Characteristics of vortex packets in turbulent boundary layers. *J. Fluid Mech.* **478**, 35–46.

Hutchins, N., Ganapathisubramani, B. & Marusic, I. 2004 Dominant spanwise fourier modes, and the existence of very large scale coherence in turbulent boundary layers. In *Proc. 15th Australasian Fluid Mech. Conf.* (ed. M. Behnia, W. Lin & G. D. McBain).

Hutchins, N., Hambleton, W. T. & Marusic, I. 2005 Inclined cross-stream stereo piv measurements in turbulent boundary layers. *J. Fluid Mech.* **541**, 21–54.

Jiménez, J. & del Álamo, J. C. 2004 Computing turbulent channels at experimental Reynolds numbers. In *Proc. 15th Australasian Fluid Mech. Conf.* (ed. M. Behnia, W. Lin & G. D. McBain).

Kähler, C. J. & Kompenhans, J. 2000 Fundamentals of multiple plane stereo particle image velocimetry. *Exps. Fluids* **29**, 70–77.

Kiger, K. T. & Pan, C. 2002 Suspension and turbulence modification effects of solid particles on a horizontal turbulent channel flow. *J. Turbulence* **3(019)**, 1–21.

Kim, K. C. & Adrian, R. J. 1999 Very large-scale motion in the outer layer. *Phys. Fluids* **11**, 417–422.

Kim, K. C. & Kwon, S. H. 2004 Three-dimensional topology of hairpin packet structure in turbulent boundary layer. In *12th Intl. Symp. Applic. Laser Techn. Fluid Mech*. Lisbon, Portugal.

Klewicki, J. C. 1997 Self-sustaining traits of near-wall motions underlying boundary layer stress transport. In *Self-Sustaining Mechanisms of Wall Turbulence* (ed. R. L. Panton). Computational and Mechanical Publications.

Kovasznay, L. S. G., Kibens, V. & Blackwelder, R. F. 1970 Large-scale motion in the intermittent region of a turbulent boundary layer. *J. Fluid Mech.* **41**, 283–326.

Lewkowicz, A. K. 1982 An improved universal wake function for turbulent boundary layers and some of its consequences. *A. Flugwiss. Weltraumforsch* **6**, 261–266.

Marusic, I. 2001 On the role of large-scale structures in wall turbulence. *Phys. Fluids* **13**, 735–743.

Perry, A. E. & Marusic, I. 1995 A wall wake model for the turbulent structure of boundary layers. Part 1. Extension of the attached eddy hypothesis. *J. Fluid Mech.* **298**, 361–388.

Raffel, M., Willert, C. & Kompenhans, J. 1998 *Particle Image Velocimetry: A Practical Guide*. Springer.

Spalart, P. R. 1988 Direct numerical simulation of a turbulent boundary layer up to $R_\theta = 1410$. *J. Fluid Mech.* **187**, 61–98.

Tomkins, C. D. & Adrian, R. J. 2003 Spanwise structure and scale growth in turbulent boundary layers. *J. Fluid Mech.* **490**, 37–74.